

Chapter 2

Structure, Stability and Electronic Properties of Nanodiamonds

Giulia Galli^{1,2}

Abstract Diamond nanoparticles, or nanodiamonds, have the most disparate origins. They are found in crude oil at concentrations up to thousands of parts per million, in meteorites, interstellar dust, and protoplanetary nebulae, as well as in certain sediment layers on Earth. They can also be produced in the laboratory by chemical vapor deposition or by detonating high explosive materials. Here we summarize what is known about nanodiamond sources; we then describe the atomic and electronic structure, and stability of diamond nanoparticles, highlighting the role of theory and computations in understanding and predicting their properties. Possible technological applications of thin films composed of nanodiamonds, ranging from micro-resonators to substrates for drug delivery, are briefly discussed.

2.1 Introduction

The properties of diamond and its practical and technological applications have been extensively investigated for centuries. Elemental carbon has been known since pre-history, and diamond is likely to have been mined in India already 2,000 years ago. But its utilization could date as far back as 6,000 years ago, as suggested by recent archaeological discoveries of diamond utensils in China [1].

In the last two decades, a ‘new’ form of diamond has attracted much attention: nanometer sized diamond particles. Such particles have been found in primitive meteorites [2–4], formed before the solar system, in proto-planetary nebulae and in interplanetary dust [5], as well as in several earth sediments dated around 13,000 calendar years before present (B.P.) [6, 7]. The study of the origin and formation of diamond nanoparticles in and from outer space may shed light on several problems, including the understanding of possible impacts of meteorites (carbonaceous chondrites) with our planet [7]. On the other hand, the study of the relative stability

¹Department of Chemistry, University of California, Davis, CA, USA

²Department of Physics, University of California, Davis, CA, USA
e-mail: gagalli@ucdavis.edu

of diamondoids (hydrocarbon molecules with the diamond structure, terminated by hydrogen atoms) may help assess the ultimate depth of crude-oil preservation on earth [8]. The first diamondoid (adamantane) was identified in crude oil in 1933 [9] but it was only few years ago [10] that higher molecules (with 22 C atoms or more) were recovered from oil.

In addition to geological and astrophysical interest, nanometer-sized diamonds have attracted the interest of the nanoscience and nanotechnology communities [11], for the potential application of nanodiamond films as bright, low voltage (cold) cathodes and light emitters [12], and of diamondoids as electron emitters [13, 14]. The exceptional hardness, fracture strength, and inertness of ultra-nanocrystalline diamond films, together with their smooth surface make them unique materials for miniaturized mechanical systems and devices (MEMS). Such devices include cantilevers and gears, and nanodiamond MEM devices have already been successfully produced [15]. Finally nanodiamonds are finding applications in biology as drug delivery vehicles and as substrates for DNA attachment [16].

The purpose of this brief review is to give a summary of nanodiamond sources and thin film production in the laboratory (Section 2.2), and then to focus on structural, stability and electronic properties of nanodiamonds (Sections 2.3–2.5, respectively), with the intent of highlighting the contributions of theory and computation to the understanding of these fascinating nanostructured materials.

2.2 Nanodiamond Sources

2.2.1 *Nanodiamond in and from Outer Space*

Nanoscale diamonds were discovered in 1987 by Lewis et al. [2, 3] in meteorites called carbonaceous chondrites. Two major sources of nanodiamonds are the “Allende” chondrite (C3V type), which weighed several tons when it fell on Mexico in 1969, and other types of chondrites, such as the Murchison meteorite (type C2). The nanodiamonds found in these meteorites have a lognormal size distribution, with a median diameter of about 2.5 nm, corresponding to roughly 1,100 atoms per particle. The shape of this distribution has been interpreted as stemming from a growth process in which ensembles of small grains are progressively transformed into larger ones. Meteoritic nanodiamonds were shown to contain impurities, mainly hydrogen, nitrogen, and oxygen in the form of –COOH groups. In some cases, such as in C2-type chondrites, diamond in its nanoscale form is up to five times more abundant than graphite. Additional analysis of meteoritic nanodiamonds by Amarti et al. [4] revealed the nanodiamond content of the C2 meteorite to be about 400 ppm, and the shape of the size distribution was attributed to formation by a condensation process.

An interesting question arising from Lewis’ and subsequent discoveries, concerns the origin of nanodiamonds. Daulton et al. [17] performed a detailed

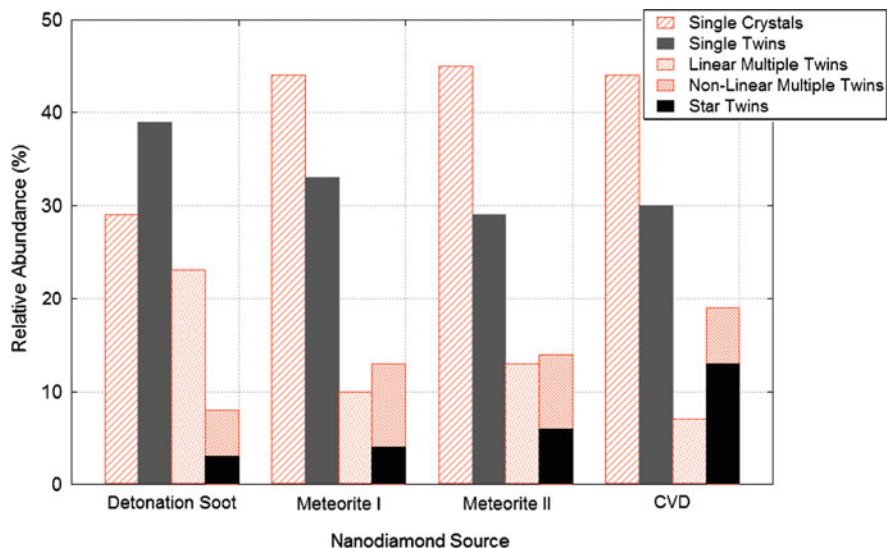


Fig. 2.1 Distribution of the different twinning types found in nanodiamonds with various origins. The meteoritic diamond [2] originated from the Murchison meteorite (I) and the Allende meteorite (II). Note the similarity between the twinning in meteoritic and Chemical Vapor Deposited (CVD) nanodiamonds. From [17]

high-resolution transmission electron microscopy (HRTEM) study of a large quantity of nanodiamonds coming from meteorites, as well as those produced by means of detonation or chemical vapor deposition (CVD) in the laboratory. They concluded that the characteristic of meteoritic nanodiamonds (morphology, type of twinning defects) are much closer to those obtained by low-hydrogen-pressure CVD than by high-temperature–high-pressure detonation, as shown in Fig. 2.1; hence they suggested that meteoritic nanodiamonds are formed by CVD-like processes, and that their growth is possibly seeded by C_{60} or C_{70} molecules. However, recently two novel formation mechanisms have been proposed, one involving diamondoid growth on ices [18] and the other one growth in dust grains [19].

Isotopic anomalies of a fraction of meteoritic diamond indicate an extra-solar source, although recent studies of Dai et al. [20] suggest that nanodiamonds might have been formed within the inner solar system. The discovery, in [20], that only minute quantities of nanodiamond is present in interplanetary dust particles (formed further out in the early Solar System than the parent asteroids from which meteorites may originate) suggests that meteoritic nanodiamond may not be presolar, consistent with data obtained from the accretion disc of young stars [21]. However the presolar origin is not ruled out by the data of Dai et al. [20], and it might still constitute a viable hypothesis; nevertheless, in this case nanodiamond abundance would be expected to decrease with heliocentric distance, a behavior that would open problems in the overall understanding of large scale transport and circulation in the early Solar system.

Nanodiamond signals have also been identified in the emission spectrum of 12 warm supergiants [22], which are carbon-rich protoplanetary nebulae. A broad absorption line from these objects, centered at 21 nm wavelength, was originally attributed to large polycyclic aromatic hydrocarbon (PAH) molecules or to some partially hydrogenated fullerenes; however, more recently Hill et al. [23] re-assigned the line to nanodiamonds. In this study, the observed infrared absorption from the interstellar dust is shown to be very similar to the signal obtained from either nitrogen-rich nanodiamonds, or nanodiamonds containing vacancies and/or interstitial atoms, produced in the laboratory. It was also noted that some absorption features could be explained by assuming that part of the nanodiamond surface attains sp^2 like configurations. By comparing the absorption spectra with those of terrestrial diamonds, Hill et al. [23] estimated the size of interstellar nanodiamonds to be around 2.5–3 nm, exactly the same size range as for meteoritic diamonds. Other indirect, nanodiamond signatures have been found by Van Kerkhoven et al. [21], originating from specific stars; those sources are thought to contain hydrogen-terminated nanoparticles, possibly exhibiting some type of surface reconstruction, and with sizes between 1 and 10 nm.

Recently nanodiamonds were found [6, 7] in the younger Dryas Boundary sediment layer at multiple locations across North America, with sizes ranging from 2 to 300 nm. Interestingly these nanoparticles have the hexagonal lonsdaleite structure and their presence is indicative of multiple air shocks and possibly surface impacts on Earth of the order of 12.9 thousand calendar years B.P. (equivalent to about 10,900 radiocarbon years B.P.).

We now turn to the discussion of nanodiamond produced in the laboratory, either by detonation or by CVD techniques.

2.2.2 Nanodiamonds in Detonation Soots and Ultra-Dispersed-Diamond (UDD) Films

Pure TNT (2,4,6-trinitrotoluene) detonation has been shown [24] to produce, among other carbon structures, nanocrystalline (NC) diamonds with diameters of about 10 nm. By mixing TNT with solids such as RDX (cyclotrimethylene trinitramine – $C_3H_6N_6O_6$), or TATB (triaminotrinitrobenzene), and by detonating the mixture in an inert gas atmosphere, spheroidal diamond particles were produced that are ~ 4 nm in diameter [25]. Following early studies, the synthesis of nanodiamonds by detonation has been optimized and detonation-produced films are now commercially available. They are often called “ultra dispersed diamond” (UDD) films because of the very narrow size distribution of the nanoparticles.

Aleksenski et al. [26, 27] performed a structural study of UDD films using X-ray diffraction and small angle X-ray scattering. They observed a diamond cluster core of about 4.3 nm, the surface of which is covered by a mixture of sp^2 - and sp^3 -bonded carbons. These authors explained their small-angle X-ray scattering (SAXS)

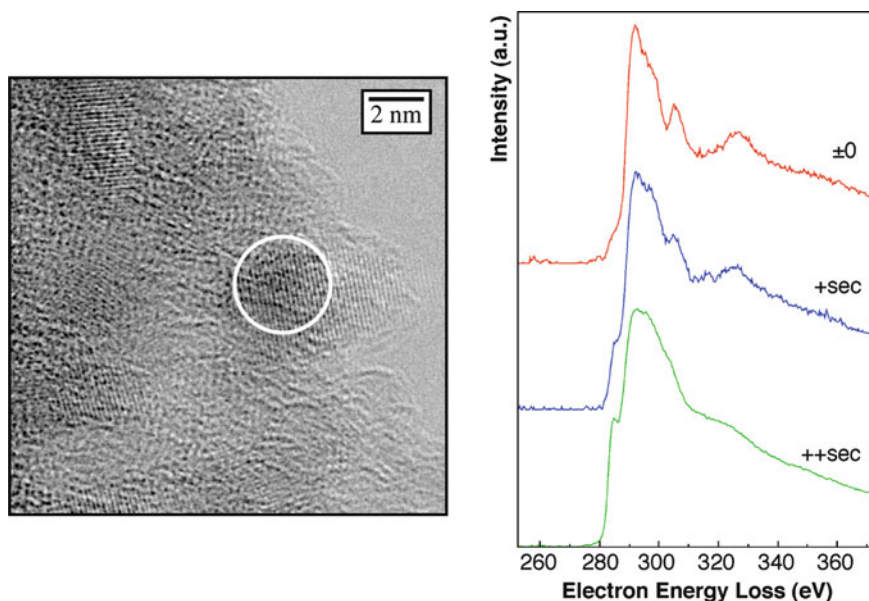


Fig. 2.2 Evolution of the electron energy loss spectrum of a Ultra-Dispersed Diamond (UDD) film (*right hand side*) as a function of the exposure time (Courtesy of T. Van Buuren and J. Plitzko, LLNL). The spectrum rapidly evolves from diamond-like to amorphous-like due to heating produced by the electron beam. A high resolution transmission electron micrograph (HRTEM) of the film is shown on the *left hand side*. A ~ 3 nm diamond nanoparticle is shown by the white circle

measurement with a model in which the diamond core is surrounded by onion-like carbon shells and nanosized graphite platelets. The thickness of these surrounding shells appears to be dependent on the type of detonation synthesis (dry technology–gas cooling, or wet technology–water cooling). Baidakova et al. [28] analyzed the fractal dimension of the external shells of nanodiamonds. Upon annealing around 1,200–1,300 K, they found that the diamond content of the nanoparticles decreases, in favor of the formation of graphite flakes on the surface. Similar transformations occur under electron beam annealing. For example, Fig. 2.2 shows the evolution of the electron energy loss spectroscopy (EELS) of a UDD film as a function of exposure time. The spectrum rapidly evolves from diamond-like to amorphous-like because of heating produced by the electron beam. Other detonation-produced (TNT+RDX) nanodiamonds were analyzed by Chen et al. [29]. In their study, the particles were almost perfectly spherical and 4–6 nm in diameter, but some larger (15 nm) particles were also detected. Their composition analysis showed 87–90% carbon, 0.5–1% hydrogen, 1.6–2.5% nitrogen, and 6–10% oxygen. These authors explained the spherical shape of the particles as a consequence of re-crystallization of liquid-like carbon droplets during the detonation, consistent with an early model proposed by Viccelli et al. [30]. The structure was shown to be diamond, with a small proportion of sp^2 -bonded carbon atoms. In UDD, small nanocrystals often

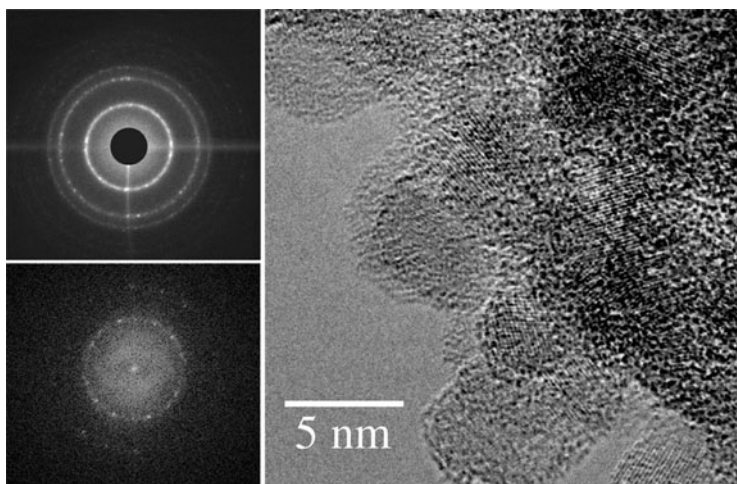


Fig. 2.3 Electron diffraction pattern (*top left*), power spectrum (*bottom left*), and a high resolution transmission electron micrograph (HRTEM) (*right*) of the edge zone of a conglomerate of nanodiamonds in Ultra-Dispersed Diamond (UDD) film (UDD). From [42]

aggregate in larger conglomerates, as shown in the study of Aleksenskii et al. [27], with small distortions of the initial spherical particle shape. A representative electron diffraction pattern is shown in Fig. 2.3.

The structure and defects of UDD have been extensively studied. In [31], infrared spectroscopy showed evidence of O–H, C–H, and C–O–C groups. Other surface groups were detected by nuclear magnetic resonance (NMR). These electron spin resonance measurements indicate that nitrogen is not present as a substitutional (paramagnetic) site inside the particle core. However, some authors [32] have measured a high concentration of paramagnetic centers in UDD films. These are attributed to dangling C–C bonds located at the interface between the diamond core and the graphene sheets forming at the surface. A similar paramagnetism has been observed in [33].

2.2.3 Nanodiamond Produced by Chemical Vapor Deposition and Ultra-Nanocrystalline Diamond (UNCD) Films

While optimizing the CVD technique for the generation of high-quality diamond films, it was found that, under some conditions, the deposited film was no longer a microcrystal assembly, but a smooth film of much smaller diamond particles [12]. A typical CVD experiment would involve the injection of a mixture of methane and hydrogen gas in a plasma reactor. The diamond film, with variable morphologies, is deposited on a silicon substrate. CVD-deposited diamonds films are distinguished into three categories [34]: microcrystalline diamonds (0.5–10 nm),

nanocrystalline diamonds (50–100 nm), and ultrananocrystalline (UNCD) diamonds (2–5 nm). Garcia et al. [35] reported diamond particles of 50 nm diameter by applying a negative d.c. bias voltage during the first minutes of the deposition from a mixture of 4% CH₄ in H₂. The nanometric diamonds appear to represent the first stage of diamond growth, as long deposition times show them coalesce to form a micro-crystalline diamond film. Nanocrystalline diamond crystals with a typical size of 50–100 nm are produced by hollow cathode arc plasma CVD, or direct current glow discharge-assisted CVD, among many other experiments.

Gruen et al. [12] devised a procedure to optimize the gas concentration to generate UNC diamonds. Replacing the majority of hydrogen by argon (typical 1% hydrogen) in the plasma yields the deposition of a smooth film of nanoparticles of only a few nanometers in size [36]. The procedure has been perfected over the years and now UCND films for several applications, e.g. for MEMS are available [15]: an example is shown in Fig. 2.4. These UNCD films contain only 2–5% of sp²-bonded carbons in grain boundaries and less than 1% hydrogen. In other cases [37] a detailed analysis of the proportion of nanodiamonds to graphite has shown that up to 75% of carbon present in the film is sp³-bonded carbon, in 3- to 5-nm diamond nanocrystals. The remaining sp²-bonded atoms are likely to be mostly present in the form of a thin graphite layer (150–200 nm) located between the substrate and the UNCD diamond, as well as in grain boundaries. An extensive review of UCND films is given in [12].

In the next session we describe nanometer-sized diamond particles and smaller molecules with a diamond cage, in which the surface is perfectly passivated by hydrogen atoms.

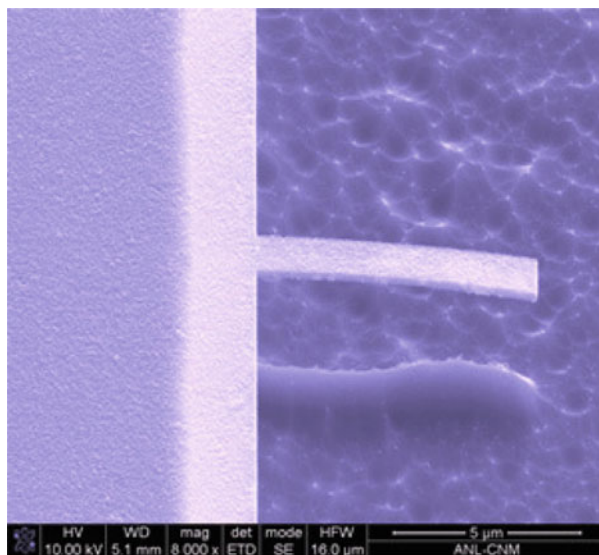
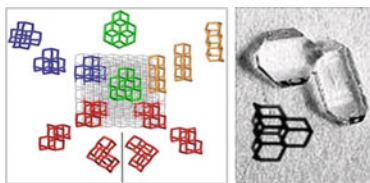


Fig. 2.4 Scanning Electron micrograph (SEM) of a micro-resonator fabricated from ultrananocrystalline diamond films at Argonne National Laboratory. The procedure is described in [15]; the figure is from: http://nano.anl.gov/news/highlights/2009_microresonators.html

Fig. 2.5 Screw-shaped higher diamondoids (*left hand side*) and an image of the pentamantane crystal (*right hand side*). Adapted from [10]



2.2.4 Nanodiamond in Oil: Diamondoids

As mentioned in the introduction, diamondoids are molecules consisting of diamond cages terminated by hydrogen atoms, as shown in Fig. 2.5. The first molecule in the series is adamantane ($C_{10}H_{16}$), discovered in 1933 [9], followed by di- ($C_{14}H_{20}$), tri- ($C_{18}H_{24}$), tetra- ($C_{22}H_{28}$) amantane and so on. These molecules are difficult to synthesize in the laboratory [8, 38] and small traces have been found in petroleum [10, 39, 40] and interstellar gases [5] over decades. In fact both neutral and cationic forms may be present in certain interstellar gases, as recently suggested by theoretical calculations of infrared spectra [5].

The high chemical stability of diamondoids has prompted their use in coal liquefaction studies and as matrices for free-radical reactions. In the Earth, diamondoids outlive other hydrocarbon found in crude oils and it has been suggested that their stability may be used to assess the ultimate depth of crude oil preservations [8].

A major breakthrough in isolating diamondoids in natural gas was made in 2003 [10], and it was also shown that these molecules could be functionalized with several groups, thus increasing their ability to, e.g. stick to surfaces, as achieved in recent experiments [14]. Before experiments probing diamondoids on surfaces, first principles calculations [13, 41] suggested that these hydrogenated carbon clusters are very different from their Si and Ge counterparts and, in particular, that they should exhibit negative electron affinity. Subsequent experiments have confirmed the picture suggested by *ab initio* calculations. In particular the first experiments of electron emission properties of layers of diamondoids on metal surfaces were recently reported [14]. These diamondoid layers could have interesting applications, e.g. as constituents of low power consumption flat panel displays. Their electronic properties will be discussed in detail in Section 2.5.

2.3 Structural Properties of Nanodiamonds

The crystallinity of a variety of nanodiamond samples has been verified by diffraction experiments, and it has also been directly observed by electron microscopy (see, e.g. enhanced atomic planes in Figs. 2.2 and 2.3). A detailed crystallographic study of nanodiamonds found in meteorites, detonation soots, and CVD grown UNC films has been performed, e.g. by Daulton et al. [17] who have reported the presence

of twinning defects in most nanoparticles, in different forms (see Fig. 2.1). Overall, the shape of nanodiamonds has been found to be close to spherical.

While the core of diamond nanoparticles is well characterized and there are little doubts about the presence of a diamond cage, the structure of nanodiamond surfaces is more controversial, as it is much more difficult to characterize experimentally. The presence of hydrogen atoms at the surface appear to be dependent on preparation conditions and will be discussed in more detail in Section 2.4. If hydrogen is not present at the surface, both computer simulations and experiments [26, 27, 42] suggest that graphitic like reconstructions and onion-like structures appear at the surface of nanodiamonds.

In particular, first principles calculations have found fullerene-like reconstructions in the 2–4 nm size range, leading to nanoparticles that have a hybrid structure [42]; these nanoparticles have been called *bucky-diamonds*. Two bucky diamonds as obtained using *ab initio* simulations and that of a larger one studied with semi-empirical tight-binding methods are reported in Fig. 2.6. We note that the predicted reconstruction induces an effective tensile stress acting on the core of the nanocluster: this effect is at variance with the one found in Si and Ge dots where surface reconstruction induces an effective compression on the nanoparticle core [43]. On the contrary, calculations carried out with empirical potentials (Brenner potential) by Halicioglu et al. [44] found inward relaxation from the top surface layers, the interatomic distance between neighboring atoms decreasing from the center of the cluster to the surface. In *ab-initio* simulations, the barrier between the ideal surface structure and the reconstructed surface found in bucky diamond is size dependent and increases as the size of the nanoparticle is increased, to become of the order of several tens of an eV, as found in bulk diamond [45]. The comparison between *ab initio* calculations and measured XAS spectra of UDD films [42] indicates that the surface reconstruction of nanodiamond identified by computer simulations is responsible for pre-edge, graphitic-like features observed in absorption spectra. These are shown in Fig. 2.7.

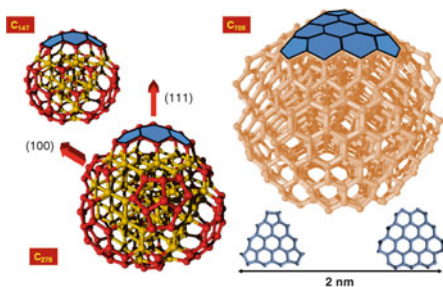


Fig. 2.6 Ball and stick representation of bare nanodiamonds (*bucky-diamonds*) composed of a diamond core (*yellow spheres*) and graphitic-like surfaces (*red spheres*). Some of the reconstructed facets on top of the diamond core are highlighted (*blue*) for clarity. They consist of a mixed pentagon/hexagon network, as represented in the lower *right hand side* of the figure

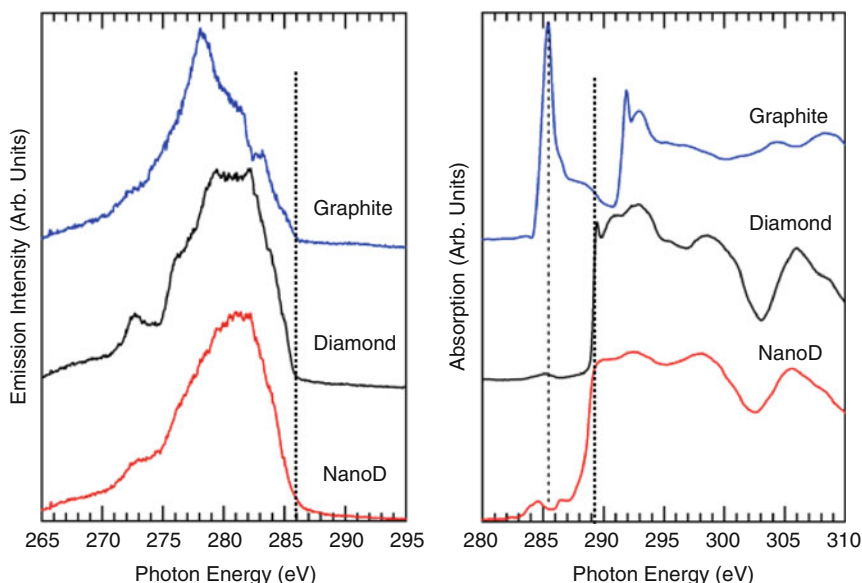


Fig. 2.7 Emission (*left panel*) and absorption (*right panel*) spectra of nanodiamond (*red line*) compared to bulk diamond and highly oriented pyrolytic graphite. From [42]

2.4 Stability of Nanodiamonds

The first attempt to understand the stability of diamonds at the nanoscale was reported by Badziag et al. [46]. These authors computed the binding energy of diamond-like and graphite-like carbon clusters using fixed energy values for carbon–carbon and carbon–hydrogen bonds. They found that below a size of 3–6 nm, diamond clusters become more stable than their graphitic counterparts. After the study of Ref. [46], several groups provided models of the relative stability of diamond and graphite like nanoparticles, with different levels of sophistication. Charged cluster models were presented by Hwang et al. [47] and Jang and Hwang [48], and the crossover between diamond and graphite was predicted to occur for clusters containing 400 atoms. Other charge lattice calculations by Gamarnik [49] predicted instead a reversal of stability between diamond and graphite to occur between 4.3 and 10.2 nm, depending on the temperature. It is worth noting that although these models are based on totally different approximations and neglect the detailed structure of the clusters, such as specific surface reconstructions or degrees of hydrogen passivation, they all reach similar conclusions, namely that nanodiamond becomes more stable than nano-scale graphite below 3–10 nm.

A remarkable property of nanodiamonds produced under different conditions of atmosphere, temperature, and pressure is that most of them have similar size distributions. In particular, extraterrestrial nanodiamonds, some detonation nanodiamonds, and ultrananocrystalline diamonds have sizes that typically range between 2 and 5 nm.

The range of stability of nanodiamond and the reason why diamond is ultra-dispersed at the nanoscale was addressed in Ref. [50] by using first principles calculations [51,52]. In particular, the relative stability of nanodiamonds as a function of size and of the surface hydrogen coverage, in going from a totally passivated surface to a completely bare, fully reconstructed one, was investigated in detail. The ab initio calculations of [50] showed that as the size of diamond is reduced to about 3 nm, it is energetically more favorable for this material to have bare, reconstructed surfaces than hydrogenated surfaces. This inability to retain hydrogen at the surface may then prevent the growth of larger grains. Two ranges of hydrogen chemical potential values were identified, corresponding to two different growth conditions of diamond films: one that favors the formation of bare, reconstructed nanoparticles and thus the formation of UNCD or UDD films, the other favoring the formation of bulk diamond-like films. In the calculations, five core sizes were considered, containing 29, 66, 147, 211 and 275 C atoms; two of these are shown in Fig. 2.8; for all of the different sizes the stability sequence of the particles with different surface structures was found to be the same as a function of the hydrogen chemical potential.

Although the ab initio study of Ref. [50] could not establish the exact size at which the crossover between hydrogenated and bare, reconstructed surfaces occur, it provided a robust, qualitative explanation of why the crossover occurs in the few nanometers range, and why it is the same irrespective of preparation conditions. Based on the simple thermodynamic mechanism presented in Ref. [50], one might

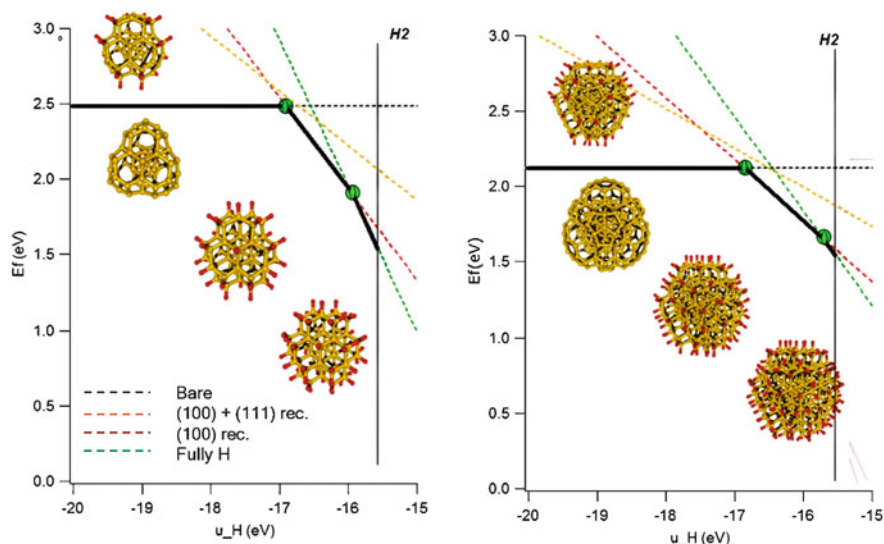


Fig. 2.8 Formation energy per carbon atom (E_f) of nanodiamonds as a function of the hydrogen chemical potential (μ_H), as obtained by first principles calculations. The nanodiamonds contain 66 (left hand side) and 275 (right hand side) C atoms. The solid black line indicates the most stable structures. From [50]

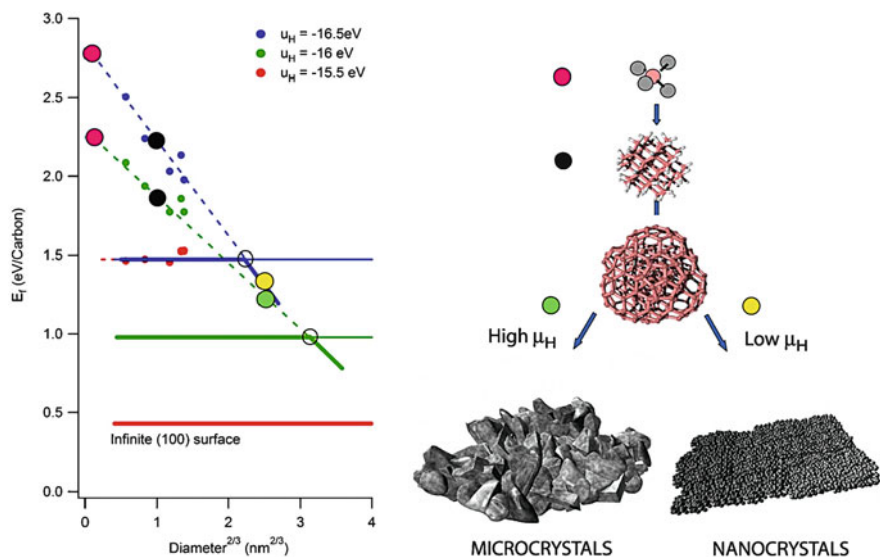


Fig. 2.9 Comparison of the formation of nanodiamonds with that of flat diamond surfaces. The *left hand side* shows the formation energy of nanodiamonds (E_f) as a function of $d^{2/3}$, where d is the particle diameter, for three values of the hydrogen chemical potential (μ_H). The formation energy of a flat (111) diamond surface for the same values of the hydrogen chemical potential, is represented by *dashed lines*. The *thick, solid lines* designate the most stable structure at any stage of a hypothetical diamond growth started from methane gas. The *right hand side* of the figure highlights the formation of different diamond films, depending on the hydrogen chemical potential conditions. From [50]

argue that it would be impossible to grow diamond on a micro- or macroscopic scale. To address this issue, it is necessary to compare the formation energies of nanodiamonds of various sizes with those of flat diamond surfaces. This comparison is shown in Fig. 2.9 where it is seen that at the highest values of the H chemical potential considered in the first principle investigation, the infinite (100) surface is more stable than any nanodiamond, while at lower chemical potential, there exist a critical diameter above which the nanodiamond clusters are the most stable structure. These numerical results helped explain how, by varying the hydrogen pressure (and thus the hydrogen chemical potential) in a CVD reactor, one can deposit either microcrystalline or ultra-nanocrystalline diamond films.

2.5 Electronic Properties of Nanodiamonds

Overall, measuring the opto-electronic properties of nanodiamond and diamondoids has proved to be challenging and has produced several controversial results. In 1999, the results of x-ray absorption near-edge structure studies of diamond films

produced by chemical vapor deposition (CVD) [53] were used to infer the evolution of the nanoparticle gap with size. This showed a persistence of quantum confinement effects up to 27 nm, a diameter surprisingly larger than in Si or Ge nanoparticles, where quantum confinement effects disappear above 5–7 nm. In contrast, recent near-edge absorption fine structure studies of diamondoids prepared by hot filament CVD [54] and high-explosive detonation waves [42] showed that quantum confinement effects disappear in particles larger than 4 nm. In particular, in [42] it was shown that there is no shift in valence and conduction band maximum and minimum in detonation nanodiamonds, in comparison with bulk diamonds. This indicates that quantum confinement does not affect the electronic structure of the measured particles, which were in the size range of 4 nm. X-ray emission and absorption spectra of detonation nanodiamonds were found to be very similar to those of bulk diamonds, with an exciton broadening (289.3 eV) and a shallower secondary minimum (302 eV) as pre-edge features. These features were attributed to specific surface reconstructions such as in bucky diamonds, as predicted by theory and described in Section 2.3. These results are consistent with those reported by Aleksenskii et al. [55] on the optical properties of UDD layers studied by optical probes and by XPS. In [55] the band gap was measured to be smaller than in diamond, 3.5 eV, and many energy levels were present in the nanodiamond band gap, contributing to a broad luminescence band (380–520 nm). The optical absorption of the material was attributed to threefold coordinated atoms on the surface.

Raty et al. [42] studied the size dependence of the optical gap of diamondoids using both time-independent and time-dependent density-functional theory [56] calculations, and concluded that quantum confinement effects disappear in nanoparticles larger than 1 nm. They also predicted that the gaps of diamondoids with sizes between 1 and 1.5 nm are *below* the gap of bulk diamond. This is strikingly different from the behavior of H-terminated Si and Ge nanoparticles [43], for which the gaps are always above the bulk band gap. In contrast, Density Functional Theory calculations by McIntosh et al. [57] for the same particles predicted optical gaps 2 eV above the gap of bulk diamond for particles ranging in size from 0.5 to 2 nm.

As discussed in detail below, highly accurate quantum Monte Carlo [58] (QMC) calculations [13] resolved this controversy, showing the disappearance of quantum confinement at about 1 nm. It was also pointed out that the results of [57] may be affected by basis set superposition errors, and these are believed to be responsible for the discrepancy between results obtained with localized and plane wave basis sets. In addition, Drummond et al. [13] predicted that diamondoids exhibit negative electron affinity. Two classes of nanoparticles were studied: (i) diamondoids constructed from adamantane cages: *adamantane*, $C_{10}H_{16}$, *diamantane*, $C_{14}H_{20}$, and *pentamantane*, $C_{26}H_{32}$; (ii) H-terminated, spherical, diamond structure nanoparticles: $C_{29}H_{36}$, $C_{66}H_{64}$, and $C_{87}H_{76}$. Because diamondoids can be extracted in large quantities from petroleum and are highly purified using high-pressure liquid chromatography, one can expect that actual experimental samples consist largely of the high-symmetry structures studied theoretically. This is not the case for Si and Ge nanoparticles, where limitations in current synthesis techniques prevent the routine production of high symmetry nanoparticles.

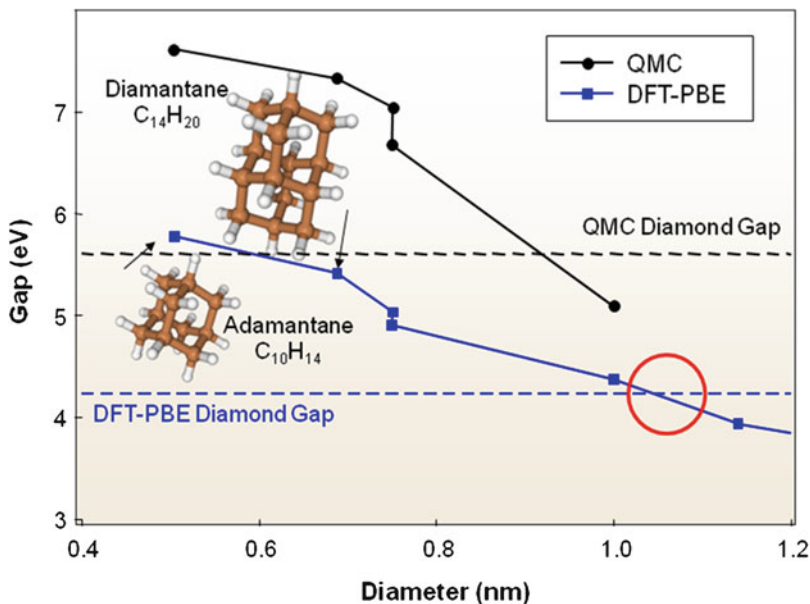


Fig. 2.10 Size dependence of the electronic gap of diamondoids as obtained using Density Functional Theory (DFT) calculations with gradient corrected exchange and correlation functionals (PBE) and Quantum Monte Carlo (QMC) calculations [13]. The *dashed blue and black lines* indicate the values of the gap of bulk diamond computed using DFT-PBE and QMC. The *red circle* indicates that at around 1 nm quantum confinement effects vanish, at both levels of theory

We first discuss the results of Density Functional Theory [51] (DFT) calculations reported in [13]. Figure 2.10 shows the size dependence of the DFT eigenvalue gap between the highest occupied molecular orbital (HOMO) and the lowest unoccupied molecular orbital (LUMO), calculated using plane-wave basis sets. The HOMO-LUMO gap decreases as the size of the nanoparticles increases. For nanoparticles larger than 1 nm, the HOMO-LUMO gap obtained with gradient corrected Density Functional Theory calculations (that we call DFT-PBE [59]) is smaller than the DFT-PBE gap of bulk diamond. It is interesting to analyze the size dependence of the individual HOMO and LUMO eigenvalues obtained from DFT (Fig. 2.11). When the size of the nanoparticles is reduced, the HOMO eigenvalue decreases continuously, as predicted by standard models of quantum confinement. In contrast, the LUMO eigenvalue displays almost no quantum confinement and is nearly independent of size. Once again, this behavior differs from that of H-terminated Si and Ge nanoparticles, in which both the HOMO and LUMO are clearly affected by quantum confinement.

The origin of the anomalous size dependence of the LUMO energy can be understood by analyzing iso-surfaces of these orbitals for specific nanoparticles: Fig. 2.12 shows the case of $C_{29}H_{36}$. The HOMO is localized on the C–C and C–H

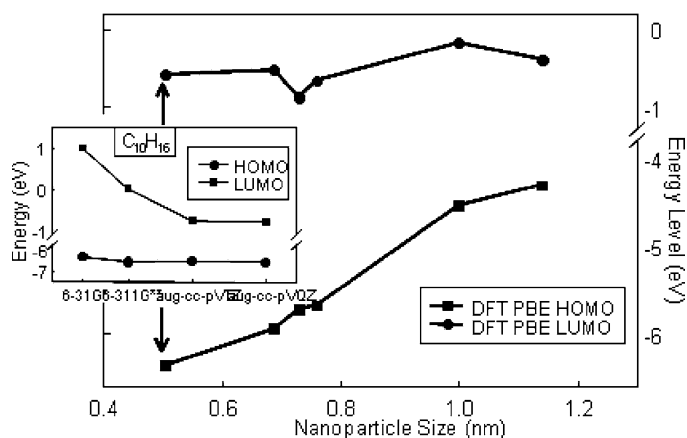


Fig. 2.11 Orbital energies of the Highest Occupied Molecular Orbital (HOMO) and Lowest Unoccupied Molecular Orbital (LUMO) of diamondoids as a function of nanoparticle size, as obtained by Density Functional Theory (DFT) calculations within the gradient corrected approximation (PBE), using plane wave basis sets. The inset shows results of DFT calculations using localized basis sets (see text). Adapted from [13]

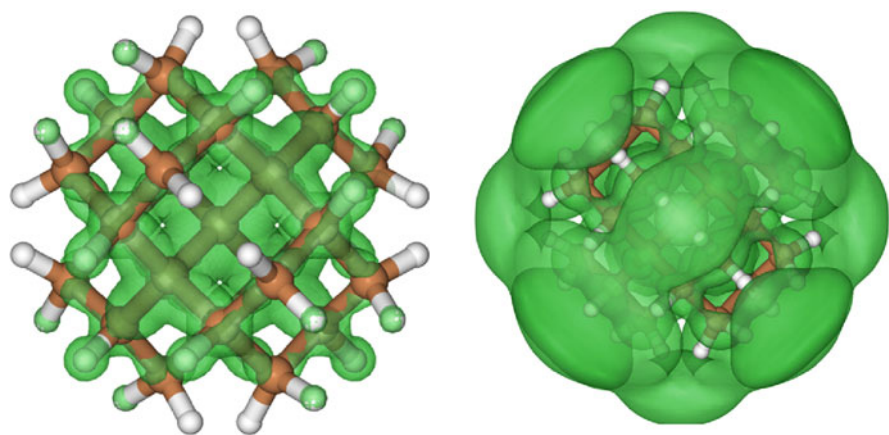


Fig. 2.12 Isosurface plots of the square of the highest occupied (*left hand side*) and lowest unoccupied (*right hand side*) orbitals of $C_{29}H_{36}$ diamondoid. The isosurfaces include 50% of the charge in each orbital. Adapted from [13]

covalent bonds inside the nanoparticle, while the LUMO is a delocalized state with considerable charge outside of the H atoms terminating the surface. As the size of the nanoparticles increases, one expects the HOMO to evolve smoothly into the valence-band maximum of bulk diamond. In contrast, for larger diamondoids, the LUMO is expected to remain in proximity of the surface, closer in nature to a defect or surface level within the gap of the bulk material; therefore the LUMO is not expected to evolve into the conduction band minimum. This surface character

of the state causes the optical gaps of the larger diamondoids to lie below the bulk gap. The delocalized nature of the LUMO as predicted by ab initio calculations was confirmed by XAS experiments [60,61].

The results of quantum monte carlo calculations (QMC) for optical gaps of the diamondoids are plotted against nanoparticle size, together with DFT results discussed above, in Fig. 2.10. QMC calculations do not suffer from the well-known DFT “band-gap problem,” as they fully describe the interaction of the valence electrons with the electron excited into the LUMO by the absorption of a photon, so that electron-hole correlation is accounted for. The QMC optical gaps are significantly larger than the DFT HOMO-LUMO gaps, as was found for Si nanoparticles [43]. For example, the QMC optical gap of $C_{10}H_{16}$ is 7.61 [2] eV, while the DFT-PBE gap is 5.77 eV. Nevertheless, the QMC results confirm the qualitative trend for the size dependence of the gap predicted by mean field theory. The QMC calculations predict that quantum confinement will be observed only in diamondoids smaller than 1 nm. This rapid decay of quantum confinement is consistent with the small exciton Bohr radius in diamond (1.6 nm), compared, e.g. to Si (4.9 nm). We note that the optical gap of $C_{66}H_{64}$ is below the bulk-diamond gap, consistent with the results of [42]. These QMC optical-gap calculations support the interpretation of the X-ray absorption measurements [42], which found no quantum confinement effects in 4 nm nanodiamonds.

First principle calculations were also applied to study the electron affinity of diamondoids. Both electron affinity (EA) and ionization potential (IP) of representative nanoparticles were evaluated at the DFT and QMC level of theory, by computing the total energy differences $EA = E_N - E_{N+1}$ and $IP = E_{N-1} - E_N$, where E_N is the ground-state energy of a neutral molecule with N electrons. In contrast to the optical gaps, where the QMC values are significantly larger than the DFT values, the QMC electron affinities agree well with the DFT values.

First principles calculations pointed at the interesting possibility of coating surfaces with diamondoids in order to produce, in a simple and economic manner, electron emitters. These predictions were recently verified experimentally [14], by depositing self-assembled monolayers (SAMs) of tetramantane-6-thiol on to a gold surface. These SAM were found to display a uniquely sharp and strong electron emission peak. Interestingly, the magnitude of this peak is much higher than that found for hydrogen-terminated diamond surfaces, that are known to exhibit a negative electron affinity (NEA). The extremely intense peak was interpreted as a signature of NEA in diamondoid SAMs. This finding indicates that nanometer-sized diamondoids may be superior to bulk diamond in electronic applications.

Not only diamondoid SAMs but also single-molecules were recently deposited on metal surfaces [62, 63]. In particular Wang et al. deposited tetramantane diamondoids on Au(111) and reported a detailed scanning tunnelling microscopy and spectroscopy study. It was shown that the diamondoid electronic structure and electron–vibrational coupling exhibit unique and unexpected spatial correlations characterized by pronounced nodal structures across the molecular surfaces.

Ab initio calculations revealed that much of the observed electronic and vibronic properties of diamondoids are determined by surface hydrogen terminations, a feature having important implications for designing future diamondoid-based molecular devices.

A very promising way to incorporate nanodiamond films in technological applications is by doping them with, e.g. nitrogen [64]. The goal is to introduce carrier levels into the diamond gap (this level is located 1.7 eV below the conduction band minimum in bulk diamonds) to increase conductivity and to lower the electron emission voltage threshold. Nitrogen is a major impurity of natural diamond. As mentioned earlier, nanodiamonds produced by detonation contain a high percentage (1–2%) of nitrogen. This nitrogen is brought into the diamonds from the trinitrotoluene reactant and cannot be removed from the nanoparticles [65]. The precise location of the nitrogen atoms in the nanoparticles is uncertain, but several magnetic studies have been unable to see any trace of substitutional nitrogen (known as P1 center) [31]. This is surprising as nitrogen is present in N-doped CVD-produced microcrystals as a substitute to core carbon atoms [66]. A theoretical study of the grain boundaries of UNC diamonds in the presence of nitrogen impurities has been performed by Zapol et al. [67]. This tight-binding, DFT study shows that nitrogen substitution to carbon in the grain boundary is energetically more favorable than in the crystalline core. The conductivity increase of the N-doped film was attributed to an increase in threefold coordinated carbon atoms caused by the nitrogen impurity. Preliminary results from ab initio molecular dynamics simulations indicate that for small diamond clusters, nitrogen is preferentially present as a substitute to surface carbon atoms. The tensile stress at the surface found in these nanoparticles facilitates nitrogen inclusion in comparison to bulk diamonds, where intentional nitrogen doping has proven to be difficult. However, nitrogen incorporation is found to require more energy with increasing particle size.

Experimentally, nitrogen doping of UNC films has been studied by Bhattacharyya et al. [68] who introduced nitrogen gas (1–20%) into the mixture fed to the CVD reactor, and achieved the highest carrier concentration and electrical conductivity measured so far for a phase-pure diamond thin film. The increase of N₂ gas concentration causes increasingly larger grain boundaries to be deposited, and it is believed to be responsible for the increase of the conductivity. However much remains to be done in order to achieve controllable doping of nanocrystalline diamond films, as well as to understand the details of the conduction mechanisms.

2.6 Conclusions and Outlook

In this brief review I have summarized structural, stability and electronic properties of nanodiamonds, and I have emphasized the role of ab initio calculations in understanding and predicting the properties of these nanoparticles. In particular I have highlighted the understanding of stability and formation in terms of

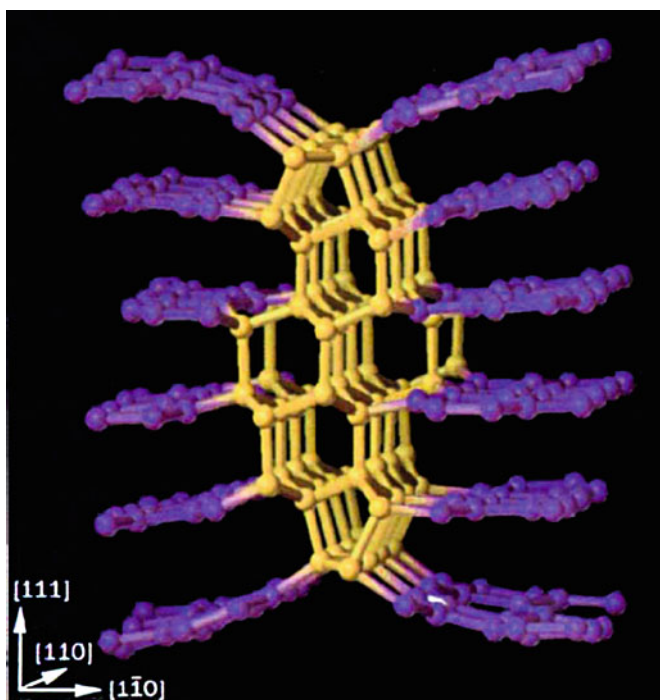


Fig. 2.13 Atomistic model of a diamond-graphite interface, as formed during graphitization of a diamond surface. Adapted from [45]

hydrogen content at the surface, and predictions about graphitic-like surface reconstructions and electronic properties. These predictions have recently been confirmed by experiments.

Of course Carbon will not stop to surprise us any time soon and new carbon based (nano)-materials are expected to be discovered and/or engineered in the future. Although the discovery of nanodiamonds is more than 20 years old and the utilization of nanodiamond films is about a decade old, certainly not all properties of these nanostructured materials have been unraveled and understood, and the general expectation is that a number of new technological applications of nanodiamonds and diamondoids lie ahead of us. Much effort is currently dedicated to another form of nanoscale Carbon: graphene and its derivatives. It will be interesting to see if nanodiamond and graphene or graphane may be combined (perhaps in a fashion similar to configurations found in diamond-graphite interfaces [45], shown in Fig. 2.13), and interfaces formed at the nanoscale. This might originate new nanoscale objects, with novel properties.

Acknowledgments This work was supported by grant No DOE/BES. DE-FG02-06ER46262

References

1. Lu PJ et al (2005) *Archaeometry* 47:1
2. Lewis RS, Ming T, Wacker JF, Anders E, Steel E (1987) *Nature* 326:160
3. Lewis RS, Anders E, Draine BT (1989) *Nature* 339:117
4. Amari S, Lewis RS, Anders E (1994) *Geochim Cosmochim Acta* 58:459
5. Bauschlicher CW, Liu YF, Ricca A, Mattioda AL, Allamandola LJ (2007) *Astrophys J* 671:458
6. Kennett DJ et al (2009) *Science* 323:94
7. Kennett DJ et al (2009) *Proc Natl Acad Sci USA* 106:12623
8. Schoell M, Carlson RMK (1999) *Nature* 399:15
9. Landa S, Machacek V (1933) *Collect Czechoslovakian Chem Commun* 5:1
10. Dahl JE, Liu SG, Carlson RMK (2003) *Science* 299:96
11. Drummond ND, *Nat Nano* (2007) 2:462
12. Shedorova OA, Gruen DM (ed) (2006) *Ultrananocrystalline diamond: synthesis, properties, and applications*. William Andrew Publishing, Norwich, NY
13. Drummond ND, Williamson AJ, Needs RJ, Galli G (2005) *Phys Rev Lett* 95:096801
14. Yang WL et al (2007) *Science* 316:1460
15. Adiga VP et al (2009) *Phys Rev B* 79:245403
16. Shimkunas RA et al (2009) *Biomaterials* 30:5720
17. Daulton TL, Eisenhour DD, Bernatowicz TJ, Lewis RS, Buseck PR (1996) *Geochim Cosmochim Acta* 60:4853
18. Kouchi A, Nakano H, Kimura Y, Kaito C (2005) *Astrophys J Lett* 626:L129
19. Freund MM, Freund FT (2006) *Astrophys J* 639:210
20. Dai ZR et al (2002) *Nature* 418:157
21. Van Kerckhoven C, Tielens A, Waelkens C (2002) *Astronom Astrophys* 384:568
22. Buss RH et al (1990) *Astrophys J* 365:L23
23. Hill HGM, Jones AP, d'Hendecourt LB (1998) *Astronom Astrophys* 336:L41
24. Vanthiel M, Ree FH (1987) *J Appl Phys* 62:1761
25. Greiner NR, Phillips DS, Johnson JD, Volk F (1988) *Nature* 333:440
26. Aleksenskii AE, Baidakova MV, Vul AY, Siklitskii VI (1999) *Phys Solid State* 41:668
27. Aleksenskii AE et al (2000) *Technic Phys Lett* 26:819
28. Baidakova MV, Siklitsky VI, Vul AY (1999) *Chaos Solitons Fractals* 10:2153
29. Chen PW, Ding YS, Chen Q, Huang FL, Yun SR (2000) *Diamond Related Mater* 9:1722
30. Viecelli JA, Bastea S, Glosli JN, Ree FH (2001) *J Chem Phys* 115:2730
31. Iakubovskii K et al (2000) *Diamond Related Mater* 9:861
32. Shames AI et al (2002) *J Phys Chem Solid* 63:1993
33. Beloborv P, Gordeev A, Petrakovskaya E, Falaleev O (2000) *Doklady Phys* 46:459
34. Fayette L et al (1998) *Phys Rev B* 57:14123
35. Garcia MM et al (1998) *Appl Phys Lett* 72:2105
36. Jiao S et al (2001) *J Appl Phys* 90:118
37. Heiman A et al (2001) *J Appl Phys* 89:2622
38. McKervey MA (1980) *Tetrahedron* 36:971
39. Dahl JE et al (1999) *Nature* 399:54
40. Lin R, Wilk ZA (1995) *Fuel* 74:1512
41. Drummond ND, Williamson AJ, Needs RJ, Galli G (2005) *Phys Rev Lett* 95:096801
42. Raty JY, Galli G, Bostedt C, van Buuren TW, Terminello LJ (2003) *Phys Rev Lett* 90:037401/1
43. Williamson AJ, Grossman JC, Hood RQ, Puzder A, Galli G (2002) *Phys Rev Lett* 89:196803
44. Halicioglu T (1997) *Phys Status Solidi B Basic Res* 199:345
45. De Vita A, Galli G, Canning A, Car R (1996) *Nature* 379:523
46. Badziag P, Verwoerd WS, Ellis WP, Greiner NR (1990) *Nature* 343:244
47. Hwang NM, Hahn JH, Yoon DY (1996) *J Crystal Growth* 162:55
48. Jang HM, Hwang NM (1998) *J Mater Res* 13:3536
49. Gamarnik MY (1996) *Phys Rev B* 54:2150
50. Raty JY, Galli G (2003) *Nat Mater* 2:792

51. Kohn W, Sham LJ (1965) *Phys Rev A* 140:1133
52. Car R, Parrinello M (1985) *Phys Rev Lett* 55:2471
53. Chang YK et al (1999) *Phys Rev Lett* 82:5377
54. Tang YH et al (2003) *Chem Phys Lett* 372:320
55. Aleksenskii AE et al (2001) *Phys Solid State* 43:145
56. Runge E, Gross EKV (1984) *Phys Rev Lett* 52:997
57. McIntosh GC, Yoon M, Berber S, Tománek D (2004) *Phys Rev B* 70:045401
58. Towler MD, Hood RQ, Needs RJ (2000) *Phys Rev B* 62:2330
59. Perdew JP, Burke K, Ernzerhof M (1996) *Phys Rev Lett* 77:3865
60. Willey TM et al (2005) *Phys Rev Lett* 95:113401
61. Willey TM et al (2006) *Phys Rev B (Condensed Matter and Materials Physics)* 74:205432
62. Wang Y et al (2008) *Nat Mater* 7:38
63. de Lozanne A (2008) *Nat Mater* 7:10
64. Achatz P et al (2006) *Phys Rev B (Condensed Matter and Materials Physics)* 74:155429
65. Maillard-Schaller E et al (1999) *Diamond Related Mater* 8:805
66. Nokhrin S, Rosa J, Vanecek M, Badalyan AG, Nesladek M (2001) *Diamond Related Mater* 10:480
67. Zapol P, Sternberg M, Curtiss LA, Frauenheim T, Gruen DM (2001) *Phys Rev B* 65:045403
68. Bhattacharyya S et al (2001) *Appl Phys Lett* 79:1441

Computer-Based Modeling of Novel Carbon Systems
and Their Properties

Beyond Nanotubes

Colombo, L.; Fasolino, A. (Eds.)

2010, VIII, 250 p., Hardcover

ISBN: 978-1-4020-9717-1